International Journal of Research in Advance Engineering, (IJRAE)
Vol. 2, Issue 5, Sep-Oct-2016, Available at: **www.knowledgecuddle.com/index.php/IJRAE**

Enhancement of Discharge Capacity of Mg/MnO_2 Primary Cell with Nano-MnO_2-Graphene as Cathode

Narthana K[1], Naveen kumar R[1], K. Saminathan[1], P. Siva[1], M. Selvam[1*] and P. Saha[2]

[1]Centre for Nano Science and Technology, KS Rangasamy College of Technology,
Tiruchengode – 637 215, Tamil Nadu, India

[2]Department of Ceramic Engineering, National Institute of Technology, Rourkela, Odisha-769008, India

Abstract: **In the present study, pristine □-MnO_2 and graphene mixed with nanoparticles □-MnO_2-based cathode were prepared and their electrochemical performances were studied in a magnesium/ manganese dioxide-graphene (Mg/□-MnO_2-graphene) primary battery cell. A modified Mg/MnO_2-graphene primary cell was constructed using the prepared α-MnO_2 nanoparticles [Sample A (α-MnO_2) and Sample B (α-MnO_2-graphene)] and electrochemically synthesized graphene in a Swagelok type cell. The discharge measurements of the modified Mg/MnO_2 cell were analyzed using galvanostatic constant current (1, 5 and 10 mA) discharge with the cutoff voltage of 0.2V. The discharge capacity of α-MnO_2 based cathode was 20, 46 and 73 $mAhg^{-1}$ respectively at 1, 5, 10 mA constant current, respectively. Similarly the discharge capacity of α-MnO_2-graphene based cathode was 68, 308 and 271 $mAhg^{-1}$, respectively. Moreover, the discharge capacity of cathode based on α-MnO_2-graphene increased three times compared to α-MnO_2 based electrode. The present work unveils that graphene-□-MnO_2 based cathode is suitable for primary magnesium battery application.**

Keywords: Nanoparticles, Graphene, Cathode Material, Discharge Capacity, Modified Mg/MnO_2 Primary Cell.

I. INTRODUCTION

Currently, different form of nanostructures enables numerous applications such as electronics, sensors, memory storage, biomedical, and energy storage and conversion [1]. In particular; manganese dioxide- based nanomaterials are widely used in supercapacitors and rechargeable batteries to provide good capacitive performance for energy storage applications when compared with the conventional products [2–4]. Energy-efficient technologies and long-lasting batteries are the most crucial requirements in today's consumer electronic devices [5]. In the way, primary batteries can provide electric current immediate for compact electric and electronic devices [6]. Generally, a conventional cell, *viz.* Mg/manganese dioxide (Mg/MnO_2) primary batteries, is well known because of their acceptable performance characteristics for a large number of applications, low cost and ready availability [7-10].

Recently, carbon-based electrode materials have found wide use in energy storage and conversion process because of their unique properties. Particularly, porous carbon materials such as mesoporous carbon, activated carbon, carbon fibers, and carbon nanotubes have been successfully used as an electrode in electrical double-layer capacitors (EDLC) and pseudo-capacitors (PC) [2]. These materials exhibit high electrical conductivity, large surface area, good corrosion resistance, and good compatibility in composite materials with low cost. However, the usage of carbon materials in the current state is not adequate to improve the energy storage performance because of the concurrent development of electronic technology used in hybrid vehicles and electric cars. In order to overcome this problem, graphene is used as an electrode to facilitate faster ion diffusion between the materials and electrolyte [3]. Graphene is a thin planar sheet with a single-atom thickness having hexagonally arrayed two-dimensional honeycomb structure [4, 5]. Owing to their unique two dimensional structure, high surface area, remarkable chemical stability, and electrical conductivity, graphene-based materials are emerging as promising

eISSN: 2395-1648

INDEX COPERNICUS INTERNATIONAL

ICV 2014: 53.07
Standardized Value: 5.71

candidates to develop electrodes for new energy storage devices with high energy and power densities. Graphene is widely synthesized using different methods mainly to enhance its size-dependent properties. In general, methods such as epitaxial growth by ultra-high vacuum graphitization [11-13], chemical vapor deposition [14-16], solvothermal process [17, 18], sol–gels [19], and ion exchange and hydrothermal reduction [20, 21] are used to obtain graphene sheet. Among these methods, electrochemical and chemical reduction methods are widely used to synthesize graphene because of their lower cost and environment friendly nature.

Recently, magnesium (Mg) has been used as the most attractive, less toxic and eco-friendly material in the field of electrochemical energy conversion of primary and secondary batteries [22]. In primary batteries, it is used as an anode material and found suitable for magnesium/ manganese dioxide (Mg/MnO_2) batteries. Moreover, it doubles the battery capacity when compared with Zn/MnO_2 batteries [23]. The main advantages of the Mg/MnO_2 system over Zn/MnO_2 system are their higher shelf life, good capacity retention and high thermal stability [24]. However, the only drawback is the poor storage capacity; once discharged partially, it is not suitable for the long-term intermittent purposes. The electrochemical performance of the electrode material depends mainly on the surface area, structure and morphology [25]. Over the past decade, a lot of research was carried out in controlling the size, shape and structure of inorganic nanoscale materials for enhancing the physicochemical properties. Among the transition metal oxides, MnO_2 has a high theoretical capacitance of 1370 F g^{-1}. Thus, it is an attractive material for the energy storage applications. It shows different crystallographic forms such as α-, β-, λ- and *δ*-types. Basically, α-MnO_2 is a traditionally attractive material because of its specific properties for industrial applications and molecular sieves. Several techniques have been used to synthesize MnO_2 nanoparticles such as solution combustion [26], sonochemical reactions [27], microwave irradiation [28], and hydrothermal techniques. Among all the available methods, chemical reduction is the most successful method for the preparation of both the amorphous and the crystalline forms of □-MnO_2 with controlled particle size and morphology [29]. To the best of our knowledge, there have been few reports on the electrochemical behavior and reversible capacity of α-MnO_2 as an active cathode material for rechargeable Mg/MnO_2 batteries [30]. However, □-MnO_2 micron-size powders are used and compared with synthesized nanoparticles to evaluate the difference in discharge curves [31]. In addition, the electrochemical performance of the graphene-incorporated Mg/MnO_2 primary cell has yet to be explored. In this study, efforts have been made using □-MnO_2 nanoparticles as cathode material with Mg anode in modified primary cell set-up to provide a good discharge capacity and safe deeper discharge. Therefore, in this investigation, graphene sheets are obtained using electrochemical reduction methods. The prepared graphene is mixed with □-MnO_2 and prepared a composite electrode to explore its storage capacity, energy density, and its applications in energy storage batteries.

II. EXPERIMENTAL PROCEDURES

2.1. Synthesis of Graphene using electrochemical method

Analytical grade chemicals (Merck, USA) were used in this investigation without any further purification. Graphene sheets were synthesized using two approaches, namely electrochemical [32] and chemical reduction [33] methods. The electrochemical method using a potentiostatic (constant potential) technique (PGSTAT 302N; Metrohm Autolab, Netherlands) was used for the synthesis high-purity graphene. Graphite rods 6 mm in diameter (Merck; 99.6%), were used as a cathode and anode separated by a distance of 2 ± 0.1 cm in 0.01 M of poly (sodium diphenylamine sulfonate) PSDS electrolyte solution. A constant direct current (DC) potential of 6.2 V was applied across the graphite rods. During the current flow between the electrodes, the anode corroded as a black precipitate and gradually appeared in the reactor after 20 min. This black precipitate was subsequently washed with de-ionized (DI) water and ethanol. Then, the obtained supernatant was decanted. The final residue was preheated at 353 K for 24 h to obtain graphene powder [34]. The synthesized graphene powder sample is termed as electrochemical graphene (EG) sample.

The following chemical reaction involved in this process is represented in scheme 1:

Cx + PSDS + y [solv.] ⟶ Cx +PSDS] y (solv) (Scheme 1)

where Cx is graphite rods and PSDS is poly (sodium diphenyl amine) sulphonate.

eISSN: 2395-1648

ICV 2014: 53.07
Standardized Value: 5.71

2.2. Synthesis of MnO_2 Nanoparticles

Crystalline α-MnO_2 nanoparticles were prepared employing simple chemical reduction method. One gram polyvinyl alcohol (PVA) was dissolved in double-distilled water to form a homogeneous solution. Further, 2mg manganese sulfate ($MnSO_4$) was dissolved in ethanol and then added to the mixture under stirring at 353 K. Then, 1gm potassium permanganate ($KMnO_4$) aqueous solution was slowly added to the solution. After 2h of stirring, a brown colloidal solution was formed. The colloidal solution was then washed with double-distilled water and centrifuged at10, 000 rpm for 30min and subsequently dried at room temperature. The obtained residues were heat-treated at 473K for 1.5 h to obtain α-MnO_2nanoparticles [35].

$$2KMnO_4 + 3MnSO_4 + 2H_2O \longrightarrow 5\alpha\text{-}MnO_2 + K_2SO_4 + 2H_2SO_4$$

The obtained product was named as sample A. To show the particle size effect on the discharge capacity of the primary cell, another MnO_2-graphene sample (sample B) was prepared.

2.3. Materials Characterization

In order to perform the qualitative phase analysis, powder X-ray diffraction (XRD) was carried out on the powder sample using a Philips spectrometer (X'Pert-PRO; PANalytical, Netherlands), employing the CuK□□ (λ=0. 15406nm) radiation. Structural information of the powders was analyzed using Fourier transform infrared spectroscopy (Spectrum 100; PerkinElmer, USA). The spectra were collected in the range of 4000–500 cm^{-1}. Micro structural analysis of the powders was performed using scanning electron microscope (JSM-6390LV; JEOL, Japan) coupled with energy dispersive spectrometer (JED-2300; JEOL), and particle sizes were determined from a transmission electron microscope (TEM, CM200; Philips, USA).Atomic Force Microscopy provides a three dimensional profile of the surface on a nanoscale basis by measuring forces between a sharp probe (< 10 nm) and surface at very short distance (0.2-10 nm).The surface topography of coated and uncoated SS304 specimens were obtained by tapping mode imaging using atomic force microscopy (AFM, Innova, Veeco, USA). The Raman spectra of prepared EG and CG samples were obtained using a Raman spectrometer (Japan, WI Tech alpha300) confocal Raman systems equipped with an Nd: YAG laser (λ=1064 nm). The Raman spectra were recorded with a frequency of 514 nm as an excitation source using (RENISHAW M005-141, Japan) with a laser spot size of 1 μ m.

2.4 Mg/α-MnO_2-graphene Primary Cell Construction

The conventional Mg/MnO_2-graphene batteries are constructed in cylindrical forms [6]. In this study, the conventional cell set-up was modified and used to enhance discharge capacity and discharge time using the following steps:

i. The electrochemical measurements were performed by constructing an Mg/α-MnO_2- graphene primary cell (Schematic diagram in Fig.1). Here the cathode of existing conventional cylindrical (Swagelok-type) Mg-carbon battery was replaced by α-MnO_2graphene electrode. Mg metal sheet or metal powder (98%, 0.5g) was used as an anode, and it was mounted on a stainless steel (SS316L) disc.
ii. Furthermore, polypropylene separator was placed above the Mg anode 3ml of 1M $MgCl_2$ electrolyte was added to wet the separator. The cathode material was prepared by mixing α-MnO_2 nanoparticles (active material) and graphene (conductive agent) together at a ratio of 3:1 by weight to form a pellet with trace (0.1 mg) amount of poly vinylidene difluoride (PVDF).
iii. The prepared cathode was placed above the separator after wetting with an electrolyte solution. A stainless steel disc was used to pack the cathode, after which, a hollow cylindrical nylon rod was used to cover the two hemispheres. At both ends of the nylon rod, a copper cylinder was fitted to provide electrical contact. The discharge current was applied at both ends of the copper cylinder. The same procedure was used to construct the primary cell using both the samples.

2.5. Electrochemical Characterization

eISSN: 2395-1648

INDEX COPERNICUS INTERNATIONAL

ICV 2014: 53.07
Standardized Value: 5.71

The electrochemical discharge measurement of the modified Mg/□-MnO_2 and Mg/MnO_2-graphene cell was carried out using (PGSTAT 302N, Metrohm Autolab, Netherlands). The electrical discharge measurement of the constructed Mg/MnO_2 primary cell was carried out from the open circuit potential (OCP) using galvanostatic constant current discharge of 1 (C/300), 5 (C/60) and 10 mA(C/30) up to the cutoff voltage of 0.2 V. The measurement was carried out more than five time repeat trials. There was minimal variation in the result.

III. Result and Discussion

The XRD pattern of the electrochemically prepared graphene is shown in Fig. 2a. The observed peaks in the powder XRD pattern confirm the crystalline nature of the samples. A sharp intensive peak observed at diffraction angle (2θ) of 26.35° is specific to the crystalline nature of graphene sheets. The XRD pattern shows two peaks at a 2θ value of 26.35^0 and44. 35^0 for prepared graphene sample correspond to the (002) and (101). Planes (JCPDS file no. 411487) [31]. The FTIR spectra of the electrochemically synthesized graphene sample are shown in Fig. 2b. The quality of the graphene sample has been determined from the nature of vibrations occurred at corresponding bonding. A stretching, vibration peak observed at 1390 cm^{-1} may be attributed to the presence of C–C bonds, whereas the transmission bands observed at 1378 cm^{-1} and 1518 cm^{-1} correspond to C=O bonds [36]. Another sharp, but less pronounced stretching vibrational peak is due to the presence of C–C bond, which illustrates a few layer availability of carbon and the quality of bonds has been studied based on their shapes. Another weak stretching, vibration observed at 1165 cm^{-1} is considered to be due to the presence of C–O bonding, a similar behavior is observed at 1163 cm^{-1} for graphene [37]. A sharp symmetrical peak observed at 590 cm^{-1} is due to C–H bonding, which denotes the significant presence of C–H bonds in the graphene sample. Fig. 2c shows the SEM image of the as-synthesized sample of graphene particles. The surface morphology of graphene reveals the sheet/plate like structure where the particles are agglomerated. Fig. 2d shows the EDAX analysis of the as-synthesized graphene sample. EDAX analysis confirms the presence of C (83.85%) and O (14.7%) with a small trace of S (1.06%) and Si (0.39%) [8]. The detail sub-structural information of the as-prepared graphene sample is obtained from the TEM images as shown in Fig. 2e. It is evident from the bright field TEM image that graphene flakes are stacked together and reveals as a multilayered structure. It shows that the particles are aggregated with a honeycomb structure and in the order of few tens of nanometer. The interpretation of the particle size of the TEM images is difficult due to its irregular boundaries of the particles. However, the approximate particle size is measured as 20-80 nm considers the average size of particles in the TEM images. Selected-area diffraction (SAD) pattern shows the ring pattern due to the polycrystalline nature of the sample and the rings correspond to the (002) and (101) planes measured using the camera length (20 nm).Raman spectra of the prepared sample are shown in Fig. 2f. The spectrum reveals the structure of D, G, and 2D bands respectively at 1343, 1575, and 2704 cm^{-1}. The above observation confirms the existence of a graphene monolayer. Figure 2g shows an AFM image of a single graphene sheet. It appears transparent and folded over on one edge with isolated small fragments of graphene on its surface. These observations indicate the water-soluble graphene is similar to single graphene sheets peeled from pyrolytic graphite (0.9 nm thick).AFM images also confirm that evaporated dispersions of graphene oxide and graphene are comprised of isolated graphitic sheets (Figure 2g). The graphene oxide has lateral dimensions of several micrometers and a thickness of 1 nm, which is characteristic of a fully exfoliated graphene oxide sheet.

Fig. 3a shows the powder XRD pattern of the □-MnO_2 particles. The major Braggs's reflection matches with the body-centered tetragonal α-MnO_2 phase (JCPDS file no. 44-0141). The five major peaks observed at 12.7, 18.1, 28.8, 37.2, 42.1, 49.9, 56.2 and 60.3^0, 2θ value, respectively, correspond to the reflection from (110), (310), (211), (301), and (411) planes of □-MnO_2 phase. The XRD pattern confirms the crystalline nature of α-MnO_2 nanoparticles with an average crystalline size of ~20.5 nm determined using the Scherrer's formula. The FTIR spectrum of the as-synthesized α -MnO_2 powder is illustrated in Fig. 3b. The major bands observed at 693 cm^{-1} correspond to the vibrating mode; [28] at 600 cm^{-1} corresponds to the stretching mode, which involves the internal motion of a change in length of the Mn- O- Mn or Mn- O bond; [29] and the band at 537 cm^{-1} corresponds to the bending mode, which is sensitive to the Mn-O-Mn bond angle [24], In addition, band observed at 1624 cm^{-1} shows the existence of Mn trace coordinated with OH bonds., The band observed

eISSN: 2395-1648

INDEX COPERNICUS INTERNATIONAL

ICV 2014: 53.07
Standardized Value: 5.71

around 1039, 1384, 1464 and 1624 cm^{-1} shows the C-O stretching mode, C=O, C=C bending vibration and C=O symmetric bending mode, respectively. The SEM images of the prepared α-MnO_2 nanoparticles shows spherical morphology of the agglomerated particles [see Fig. 3 (c)] due to the use of polymer capping agents during synthesis. SEM-EDAX analysis shown in Fig. 3 (d) confirms the presence of Mn and O with a small trace of K. The particle morphology of the as-prepared samples are obtained from the TEM images as shown in Fig. 3e. The prepared α-MnO_2 particles are loosely connected and are composed of many small particles. The selected area electron diffraction (SAD) pattern reveals a broad doughnut shape with a few diffraction spots following a ring pattern confirm the crystalline form of the □-MnO_2 particles.

Fig. 4 shows the powder XRD pattern of the □-MnO_2 – graphene composite. The four major peaks observed in 12.7, 26.8, 37.2, and 68.1^0, 2θ value, respectively, correspond to the reflection from (001), (002), (201), and (021) planes of □-MnO_2-graphene phase. The XRD pattern confirms the crystalline nature of α-MnO_2 – graphene composite with an average crystalline size of ~42.6 nm determined using the Scherrer's formula.

3.1. Mg/MnO_2-graphene Primary Cell Discharge Measurements

The discharge measurements of the modified Mg/□-MnO_2 cell is analyzed using galvanostatic constant current (1, 5 and 10 mA) discharge from open circuit potential (OCP) with the cutoff voltage of 0.2V. Figure 5 and 6 shows the discharge curves for the Mg/□-MnO_2 primary cell fabricated using α-MnO_2 nanoparticles (samples A) and graphene mixed α-MnO_2 nanoparticles electrode (sample B) respectively. The sample A and B have an open circuit voltage of 2.1V and 2.05V, respectively. The discharge curve plotted against voltage versus time reveals a steady sloping discharge profile up to the cutoff voltage of 0.2V (38). For 1mA constant current which is discharged curve a in Fig. 4 &5 respectively, sample A shows a total discharge time of 21,626s and discharge capacity of **~20 mAh/g,** whereas, sample B shows a total discharging time of 74,246s correspond to a total discharge capacity of **~68.6 mAh/g.** It is clearly visible that sample B has a higher discharge capacity than sample A at a constant current of 1 mA. Thus, it is evident that the □-MnO_2 nanoparticles mixed with graphene electrode shows higher discharge capacity. Similarly, the discharge curve b and c shows the discharge profiles at constant current rates of 5 and 10 mA, respectively. In the discharge curve b, the sample A and B have constant current voltage (CCV) of 1.4V and 1.52V, respectively. For a constant current 5 mA, sample A shows the total discharge time 10,019s correspond to a discharge capacity of **~46 mAh/g,** whereas, sample B shows a discharge time 66,618s equivalent to discharge capacity **~308 mAh/g.** For curve c which correspond to a discharge profile at current rate 10mA, the sample A and B have OCV of 1.56V and 1.71V respectively, and. CCV value at 1.32V and 1.54 V for sample A and B. At a constant current rate of 10mA, sample A shows a total discharge time of 7886s and equivalent discharge capacity of **~73 mAh/g** and sample B discharge time of 29,349s with an equivalent discharge capacity of **~271 mAh/g.**

The excellent capacity observed in the case of □-MnO_2 mixed with graphene electrode is due to MnO_2 particles are well anchored onto the surface of graphene and incorporated between the intermediate graphene layers. □-MnO_2 was considered to be a promising electrode material for batteries due to its high theoretical capacity, low cost, environmental friendliness and natural abundance. However, the low actual capacity and the poor cyclability of □-MnO_2 due to its large volume expansion and aggregation during Mg insertion delayed its practical application [39].An effective way to solve these problems is to fabricate electrode materials by incorporating □-MnO_2 onto electrically conductive (graphene) carbon materials [40]. The conductive graphene will improve the conductivity and mitigate the poor kinetic issues observed in pristine □-MnO_2 electrode. Manganese dioxide (□-MnO_2) has been regarded as a promising active component for electrical capacitance (EC) electrodes. □-MnO_2, on the other hand, does not show good capacitance. However, graphene has been used extensively for the preparation of electrochemical capacitor electrodes, and graphene nanosheets are beginning to be challenged as a potential replacement due to their much enhanced discharge capacity. Few layers of graphene have large surface area and high electrical conductivity. So, it is expected that graphene doped with □-MnO_2 electrode will show much improved performance compare to pristine□□-MnO_2 electrode.

To exploit the potential of graphene-based materials for battery applications, in this work, we have mixed, active material (□-MnO_2) on the graphene sheet to obtain hybrid electrodes for the batteries to further increase the discharge capacity as well as the energy density while maintaining its good power performance. It is well-known, that double-layer

eISSN: 2395-1648

ICV 2014: 53.07
Standardized Value: 5.71

process involves a discharge rearrangement and related to a chemical reaction, and the double-layer capacitors have a better electrochemical stability. Accordingly, as-synthesized graphene, making more double-layer contribution compared to that of nanoparticles of □-MnO_2 owning to the presence of graphene layers; however, its electrochemical stability was obviously enhanced. Meanwhile, graphene has a better electrochemical double layer performance in strong alkaline electrolyte solution. Electrochemical properties of the □-MnO_2-graphene composite electrodes were characterized and exhibits excellent cyclic stability and good rate properties.

The discharge capacity of any electrochemical cell depends on the active surface area of the electrode [41]. When an aqueous electrolyte such as $MgCl_2$ penetrates into the electrode material through available voids/pores, it leads to an increase in the electrode–electrolyte interface area. When the particle size of the electrode decreases, the voids/pores may increase and enhance the electrode–electrolyte interface area. This in turn facilitates the free and uniform flow of $MgCl_2$ electrolyte throughout the electrode area [42]. The above studies reveal that the particle size of cathode material plays a dominant role in determining the discharge capacity of the primary cell.

The battery capacity is calculated using the following relation:

$$Q = I \times T \quad (1)$$

Where, *I* is the discharge current in amperes and *T*, the time in hours to discharge up to cutoff voltage.

The prepared sample B delivers high discharge capacity than sample A at various constant current rates. The observed high discharge capacity using graphene and nano α-MnO_2 based cathode for Mg/□-MnO_2 primary cells are due to higher Mg-ion storage capacity in the open space available in the □-MnO_2-graphene framework. Thus, the present investigation strongly suggests the usefulness of graphene-α-MnO_2-based cathode to overcome the disadvantage of losing stability after partial discharge in commercial batteries by providing safe deep discharge before disposal.

IV. CONCLUSION

In summary, a modified Mg/□-MnO_2 primary cell was constructed using □-MnO_2 nanoparticles and α-MnO_2-graphene powders. The observed peaks in the powder XRD pattern confirm the crystalline nature of the samples. A sharp intensive peak observed at diffraction angle (2θ) of 26.35° is specific to the crystalline nature of graphene sheets. It is evident from the bright field TEM image that graphene flakes are stacked together and reveals as a multilayered structure. It shows that the particles are aggregated with a honeycomb structure and in the order of few tens of nanometer. α-MnO_2 - graphene electrode shows excellent discharge capacity compared to the nanoparticle based α-MnO_2 electrode. This study confirms the usefulness of graphene as an auxiliary unit to augment the discharge capacity of Mg/□-MnO_2 based primary cell.

Figure caption

Fig.1. Schematic representation of modified Mg/□-MnO_2 primary cell set-up; (a) Swagelok cell components and (b) assembled Mg/□-MnO_2 electrochemical cell

Fig.2. Characterization of electrochemical graphene (a) XRD pattern, (b) FTIR spectra, (c) SEM image, (d) EDAX pattern, (e) TEM and SAED image pattern (inset), (f) Raman spectra, and (g) AFM image

Fig.3. Characterization of α-MnO_2 nanoparticles (a) XRD pattern (b) FTIR spectra (c) SEM image (d) EDAX pattern and (e) TEM and SAED image pattern (inset)

Fig. 4 XRD pattern of MnO_2-Graphene composite

Fig.5. Comparison of voltage *versus* capacity curve of α-MnO_2 nanoparticle cathode in a Mg primary electrochemical cell at a current rate of 1 mA (~C/300), b) 5 mA (~C/60), and c) 10 mA (~C/30)

eISSN: 2395-1648

ICV 2014: 53.07
Standardized Value: 5.71

Fig.6.Comparison of voltage *versus* capacity curve of α-MnO_2-graphene cathode in a Mg primary electrochemical cell at a current rate of 1 mA (~C/300), b) 5 mA (~C/60), and c) 10 mA (~C/30)

eISSN: 2395-1648

INDEX COPERNICUS INTERNATIONAL

ICV 2014: 53.07
Standardized Value: 5.71

REFERENCES

[1]. Soundararajan D, Kim Y, Kim JH, Kim KH, Ko JM. Hydrothermal Synthesis and Electrochemical Characteristics of Crystalline α-MnO_2 Nanotubes. Science of Advanced Materials, 2012; 4, 805.

[2]. Kim SY, Jeong S. H, Lee E. Y, Park Y. H, Bae H. C, Jang Y. S, Maeng E. H, Kim M. K, Son S. W, Skin absorption potential of ZnO nanoparticles. Toxicology and Environmental Health Sciences, 2011; 3, 258.

[3]. Zhao X, Sanchez B. M, Dobson P. J, Grant P. S, The role of nanomaterials in redox-based supercapacitors for next generation energy storage devices. Nanoscale, 2011; 3, 839-855.

[4]. Wang D, Cao L, Huang J, Wu J, Synthesis and electrochemical properties of submicron sized sheet-like LiV3O8 crystallites for lithium secondary batteries Mater. Letter, 2012; 71, 48-50.

[5]. Hiralal P, Imaizumi S, Unalan H. E, Matsumoto H, Minagawa M, Rouvala M, Nanomaterials-Enhanced All-Solid Flexible Zinc−Carbon Batteries. ACS Nano, 2010; 4, 2730-34.

[6]. Linden D, Reddy T. B, (eds.). Handbook of Batteries, McGraw- Hill, New York, 2002.

[7]. Girishkumar G, Munichandraiah N. Ageing of magnesium/manganese dioxide primary cells. Journal of Solid State Electrochemistry, 2001; 5, 8.

[8]. Ratnakumar B. V. Passive films on magnesium anodes in primary batteries. Journal of Applied Electrochemistry, 1988; 18(2), 268-279.

[9]. Ratna Kumar B. V, Sathyanarayana S. The delayed action of magnesium anodes in primary batteries Part I. Experimental studies. Journal of Power Sources, 1983; 10(3), 219–241.

[10]. Sathyanarayana S, and Ratna Kumar B. V. The delayed action of magnesium anodes in primary batteries: Part II. Theoretical studies. Journal of Power Sources, 1983; 10(3), 243–261.

[11]. Peng B, Liang J, Tao Z, Chen J. Magnesium nanostructures for energy storage and conversion. Journal of Materials Chemistry, 2009; 19, 2877.

[12]. Li C, Cheng F, Ji W, Tao Z, Chen J. Magnesium Microspheres and Nanospheres: Morphology- Controlled Synthesis and Application in Mg/MnO_2 Batteries. Nano Research, 2009; 2, 713-721.

[13]. Devaraj *S*, Gabriel *G. S*, Gajjela *S. R*, Balaya *P*. Mesoporous MnO_2 and Its Capacitive Behavior. Electrochemical and Solid-State Letters, *2012;* 15, 57-59.

[14]. Yu P, Zhang X, Chen Y, Ma Y. Solution-combustion synthesis of ε-MnO_2 for supercapacitors. Materials Letters, 2010; 64, 61-64.

[15]. Zolfaghari A, Ataherian F, Ghaemi M, Gholami A. Capacitive behavior of nanostructured MnO_2 prepared by sonochemistry method. Electrochimica Acta, 2007; 52, 2806 – 2814.

[16]. Ai Z, Zhang L, Kong F, Liu H, Xing W, Qiu J. Microwave-assisted green synthesis of MnO_2 nanoplates with environmental catalytic activity. Materials Chemistry and Physics, 2008; 111, 162.

[17]. Aravindan V, Reddy M. V, Madhavi S, Subba Rao G. V, Chowdari B. V. R. Electrochemical performance of α-MnO_2 nanorods/activated carbon hybrid supercapacitor. Nanoscience and Nanotechnology Letters, 2012; 4, 724-728.

[18]. Bao S. J, He B. L, Liang Y. Y, Zhou W. J, Li H. L. Synthesis and electrochemical characterization of amorphous MnO_2 for electrochemical capacitor. Materials Science and Engineering: A, 2005; 397, 305.

[19]. Zhang R, Yu X, Nam K. W, Ling C, Arthur T. S, Song W, Knapp A. M, Ehrlich S. N, Yang X. Q, Matsui M. α-MnO_2 as a cathode material for rechargeable Mg batteries. Electrochemistry Communications, 2012; 23, 110.

[20]. N. Tang, X. Tian, C. Yang, Z. Pi, Q. Han. Facile synthesis of α-MnO_2 nanorods for high-performance alkaline batteries. Journal of Physics and Chemistry of Solids, 2010; 71, 258 -262.

[21]. C. Yuan, B. Gao, L. Su, X. Zhang. Interface synthesis of mesoporous MnO_2 and its electrochemical capacitive behaviors. Journal of colloid and interface science, 2008; Sci. 322, 545.

[22]. P. Saha, MK. Datta, OI. Velikokhatnyi, A. Manivannan, D. Alman, PN Kumta. Rechargeable magnesium battery: Current status and key challenges for the future. Progress in Materials Science, 2014; 66, 1-86.

[23]. N.Munichandraiah. Electrochemical impedance studies of a decade-aged magnesium/manganese dioxide primary cell. Journal of Applied Electrochemistry, 1999; 29, 4, 463-471.

[24]. S. U. Kim and C. W. Monroe. Increasing the rate capability of batteries with electrolyte flow. Journal of Applied Energy, 2013; 103, 207.

[25]. SRC. Vivekchand, CS. Rout, KS. Subramanyam, A. Govindaraj, CNR. Rao. Graphene- based electrochemical super capacitors. Journal of Chemical Science, 2009; 120:9–13.

[26]. H. Wu, J. Liu, IA. Aksay, Y. Lin. Graphene based electro chemical sensors and biosensors. Journal of Electro Analytical chemistry, 2010; 22(10):1027–36.

[27]. DB. Shinde, J. Debgupta, A. Kushwaha, M. Aslam, VK. Pillai. Electrochemical unzipping of multi-walled carbon nanotubes for facile synthesis of high-quality graphene nanoribbons. Journal of American Chemical Society, 2011; 133:4168.

[28]. EJ Yoo, J. Kim, E. Hosono, HS. Zhou, T. Kudo, I. Honma. Large reversible Li storage of graphene nanosheet families for use in rechargeable lithium ion batteries. Nano Letters, 2008; 8:2277–82.

[29]. C. Wang, D. Li, CO. Too, GG. Wallace. Electrochemical properties of graphene paper electrodes used in lithium batteries. Journal of Chemical Materials, 2009; 21(13):2604–06.

[30]. Zhang et al. α-MnO_2 as a cathode material for rechargeable Mg batteries. Journal of Electrochemistry Communications, 2012; 23, 110–113.

[31]. G. Wang, B. Wang, J. Park, J. Wang, YB. Sun, J. Yao. High efficient and large-scale synthesis of graphene by electrolytic exfoliation. Carbon, 2009; 473:242–46.

[32]. M. Selvam, K. Sakthipandi, R. Suryaprabha, K. Saminathan, V. Rajendran. Synthesis and characterisation of electrochemically reduced graphene. Bulletin of Material Science, 2013; 36(7):1315–1321.

[33]. Z. Luo, Y. Lu, LA. Somers, AT. Johnson. High yield preparation of macroscopic graphene oxide membranes. Journal of American Chemistry, 2009; Soc 131(3):898–9.

[34]. M. O'Brien, B. Nichols. CVD synthesis and characterization of graphene thin films. Army research laboratory, 2010; ARL-TR- 5047.

[35]. A. Reina, X.T. Jia, LY. Ho. Large area, few-layer graphene films on arbitrary substrates by chemical vapor deposition. Nano Letters, 2009; 9(1):30–35.

[36]. A. Reina, XT. Jia, J. Ho, D. Nezich, H. Son, V. Bulovic, MS. Dresselhaus, J. Kong. Synthesis of N-doped graphene by chemical vapor deposition and its electrical properties. Nano Letters, 2009; 9(5):1752–1758.

[37]. Gopu Kumar, A. Sivashanmugam, N. Muniyandi. Para-Nitrotoluene as a depolarizer for magnesium batteries, Journal of Power Sources, 1992; 39: 1121–129.

[38]. M. Choucair, P. Thordarson, JA. Stride. Gram-scale production of graphene based on solvothermal synthesis and sonication. Nature Nanotechnology, 2009; 4:30–33.

[39]. DK. Singh, PK. Iyery, PK. Giriz. Improved chemical synthesis of graphene using a safer solvothermal route. International Journal of Nanoscience. 2011; 10(1): 1–4.

[40]. GI. Titelman, V. Gelman, S. Bron, RL. Khalfin, Y. Cohen, H. Bianco-Peled. Synthesis of water soluble graphene. Carbon, 2005; 43:641–649.

[41]. N. Liu, F. Luo, H. Wu, Y. Liu, C. Zhang, J. Chen. One-step ionic liquid- assisted electrochemical synthesis of ionic-liquid-functionalized graphene sheets directly from graphite. Advance Functional Material, 2008; 18: 1518–25.

[42]. A. Kaniyoor, T. Baby, S. Ramaprabhu. Graphene synthesis via hydrogen induced low temperature exfoliation of graphite oxide. Journal of material chemistry, 2010; 20: 8467–69.

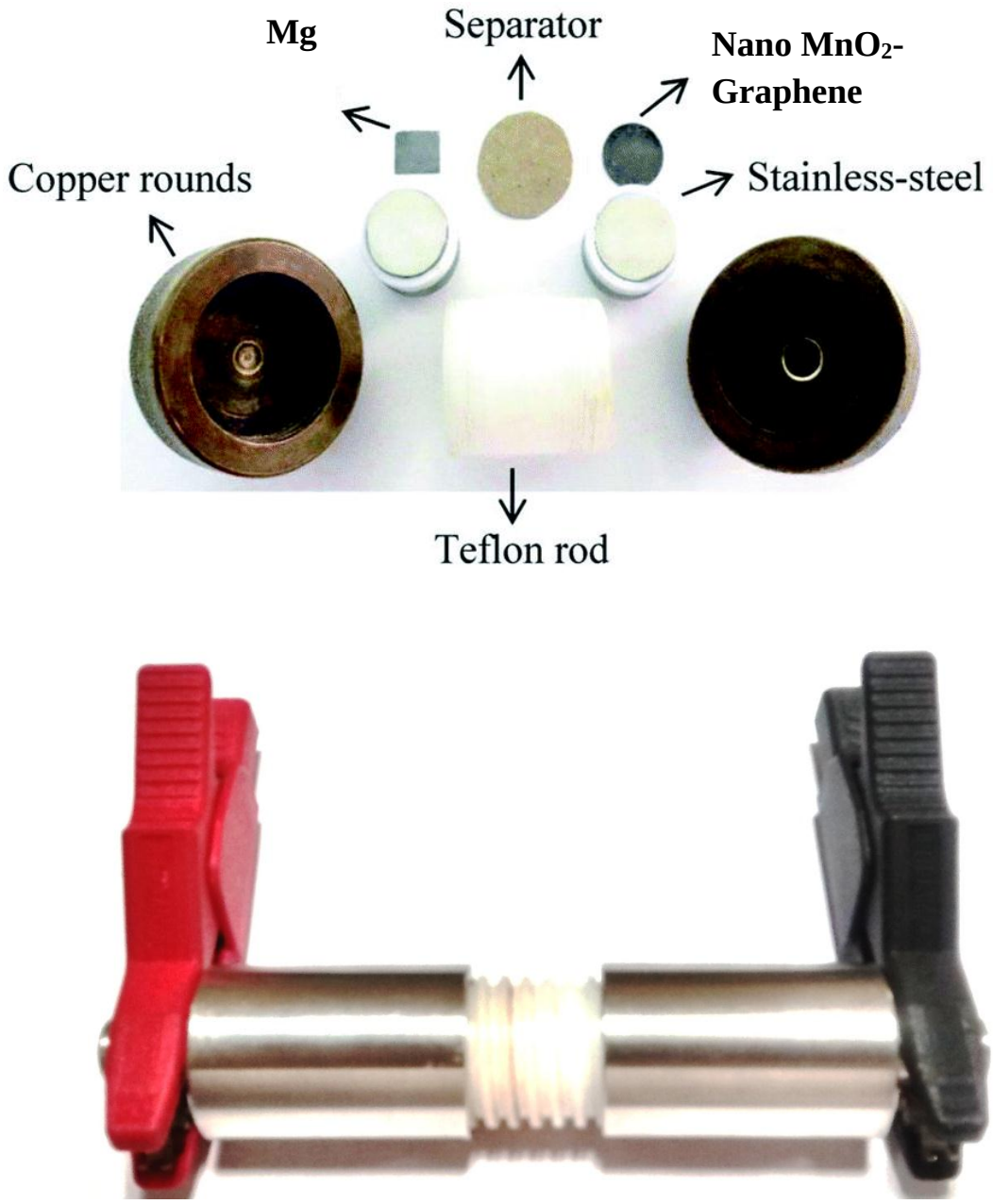

Fig. 1.Schematic representation of modified Mg/□-MnO_2 primary cell set-up. (a) Swagelok cell components and (b) assembled Mg/□-MnO_2 electrochemical cell

eISSN: 2395-1648

INDEX COPERNICUS INTERNATIONAL

ICV 2014: 53.07
Standardized Value: 5.71

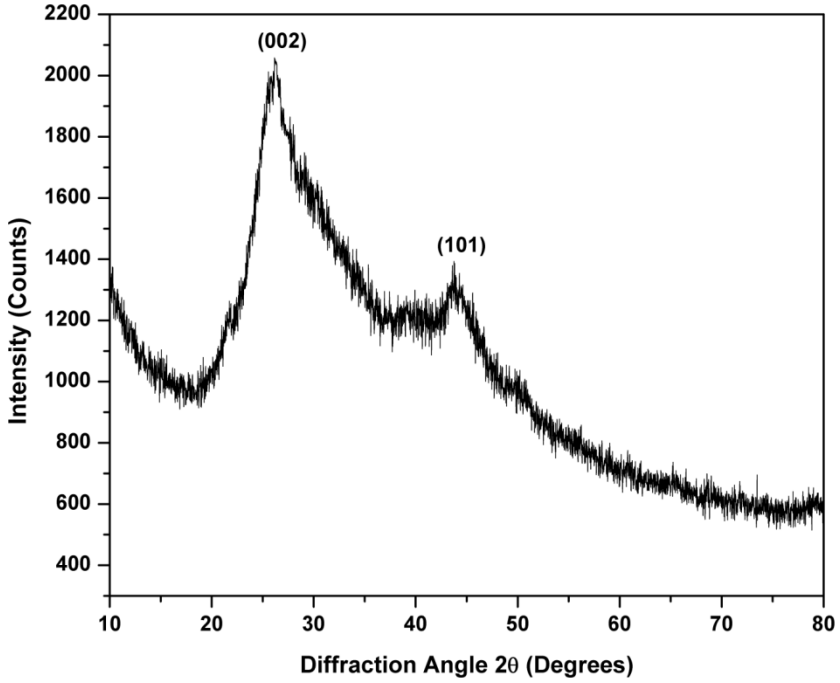

a) XRD

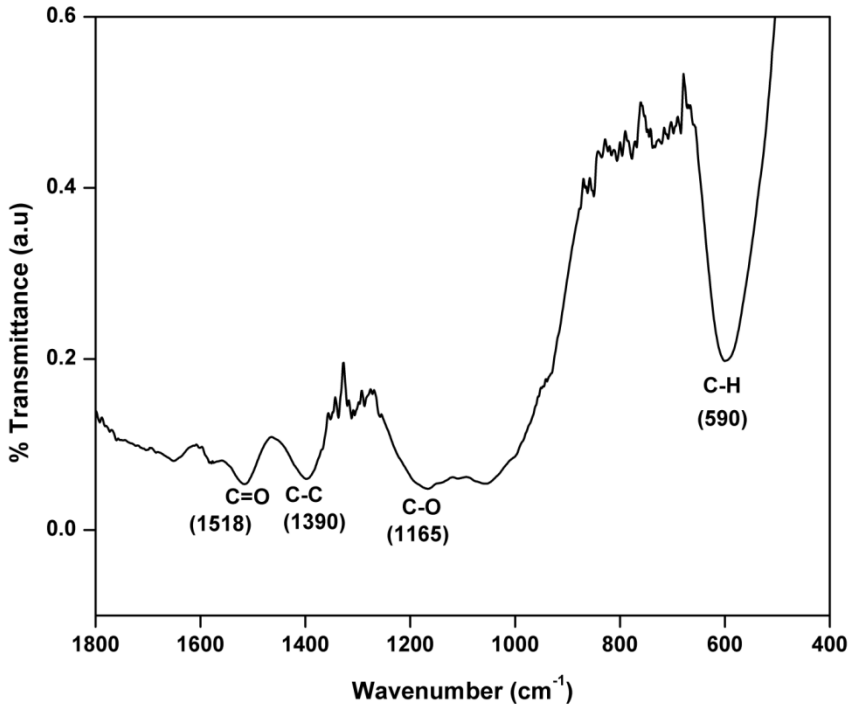

b) FTIR

eISSN: 2395-1648

INDEX COPERNICUS INTERNATIONAL

ICV 2014: 53.07
Standardized Value: 5.71

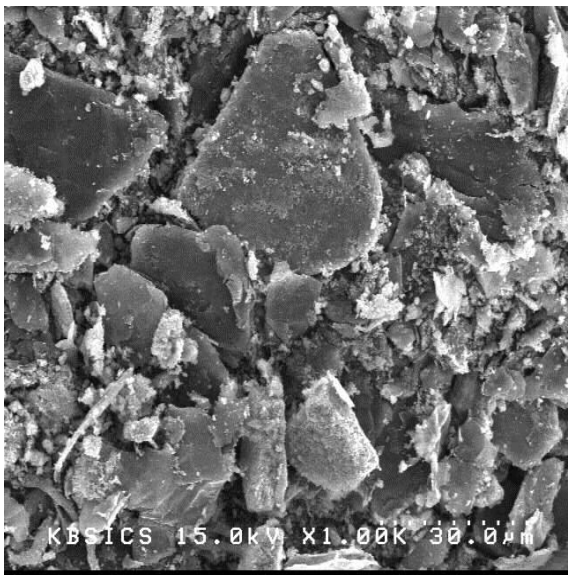

c) SEM

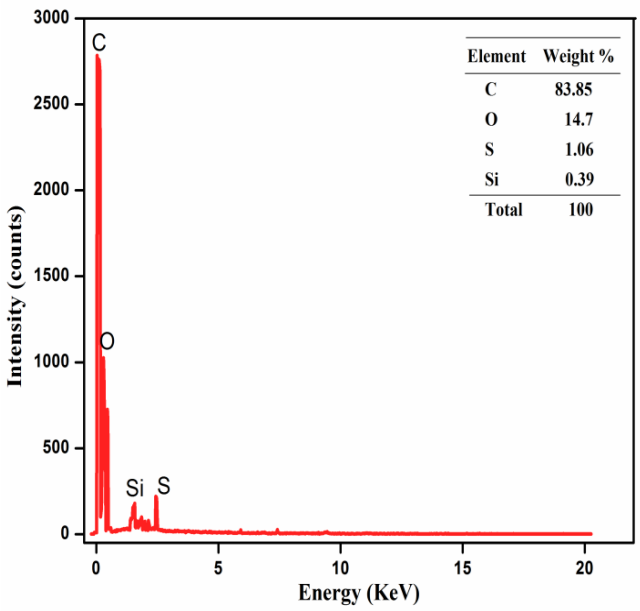

d) EDAX

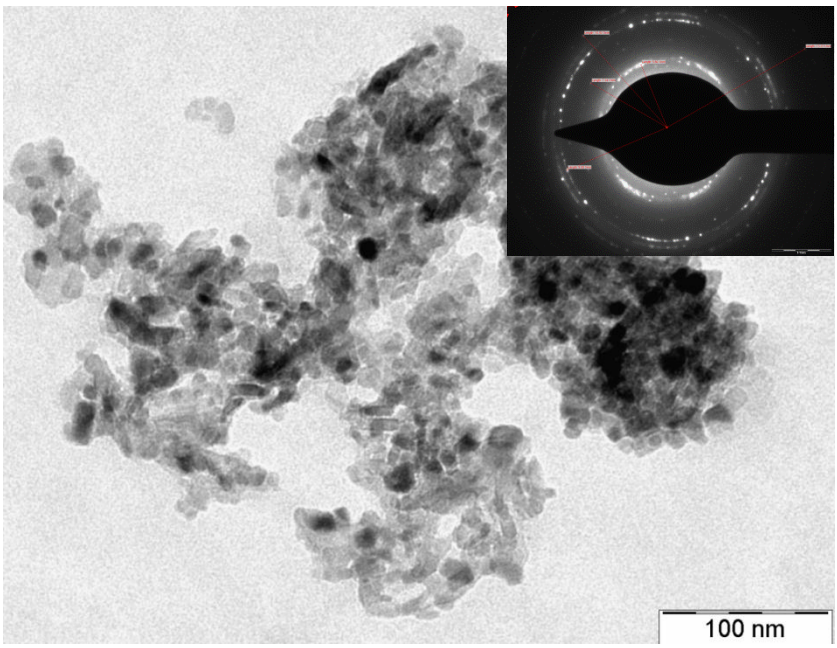

e) TEM

eISSN: 2395-1648

INDEX COPERNICUS INTERNATIONAL

ICV 2014: 53.07
Standardized Value: 5.71

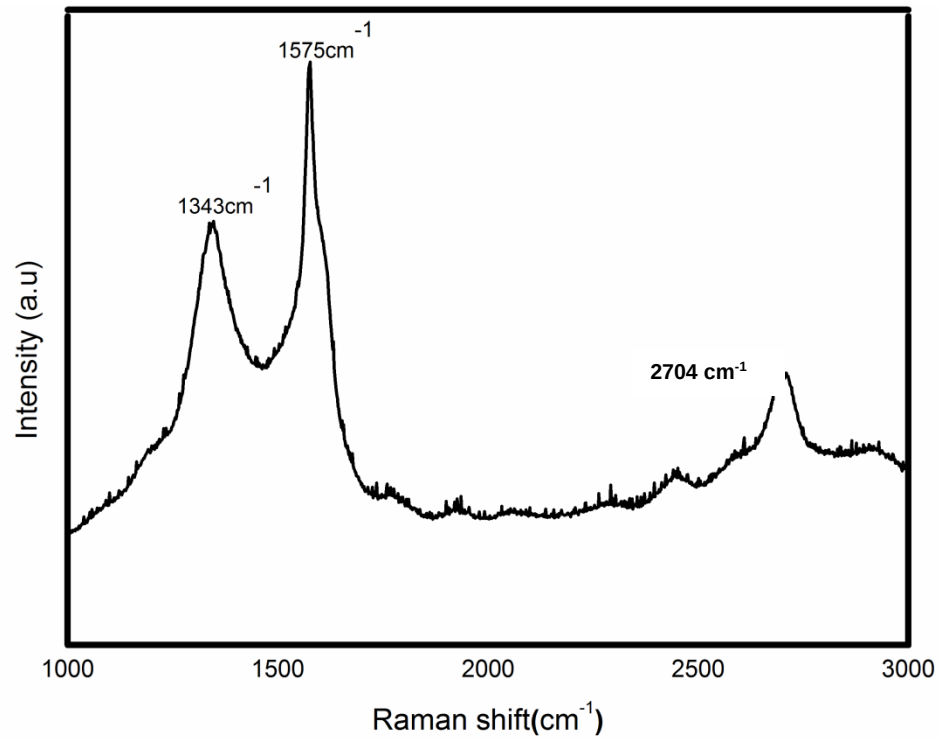

f) Raman spectra

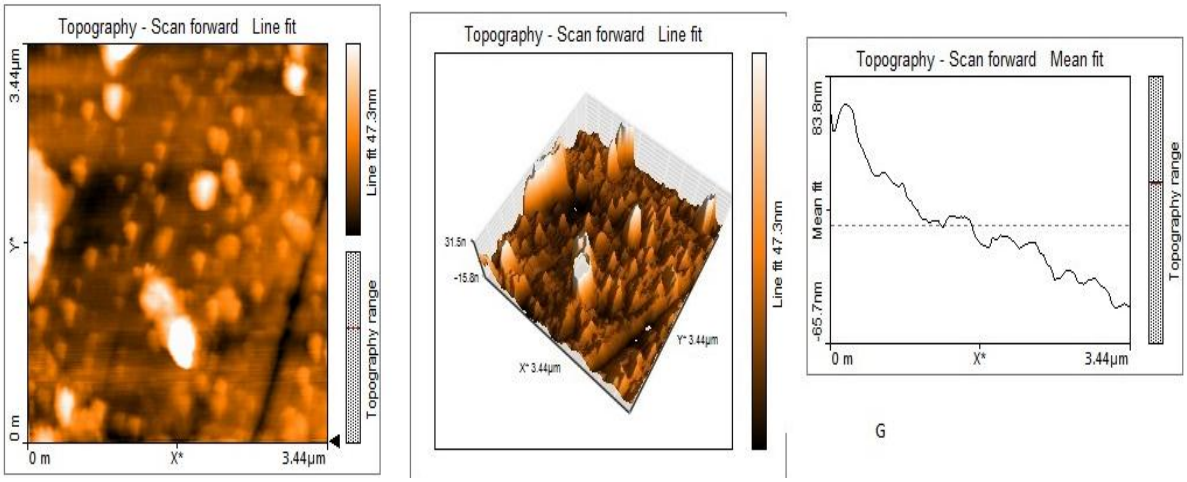

g) AFM

Fig. 2. Characterization of electrochemical graphene a) XRD pattern, b) FTIR spectra, c) SEM image, d) EDAX pattern, e) TEM and SAED image pattern (inset), f) Raman spectra and g) AFM Image

eISSN: 2395-1648

INDEX COPERNICUS INTERNATIONAL

ICV 2014: 53.07
Standardized Value: 5.71

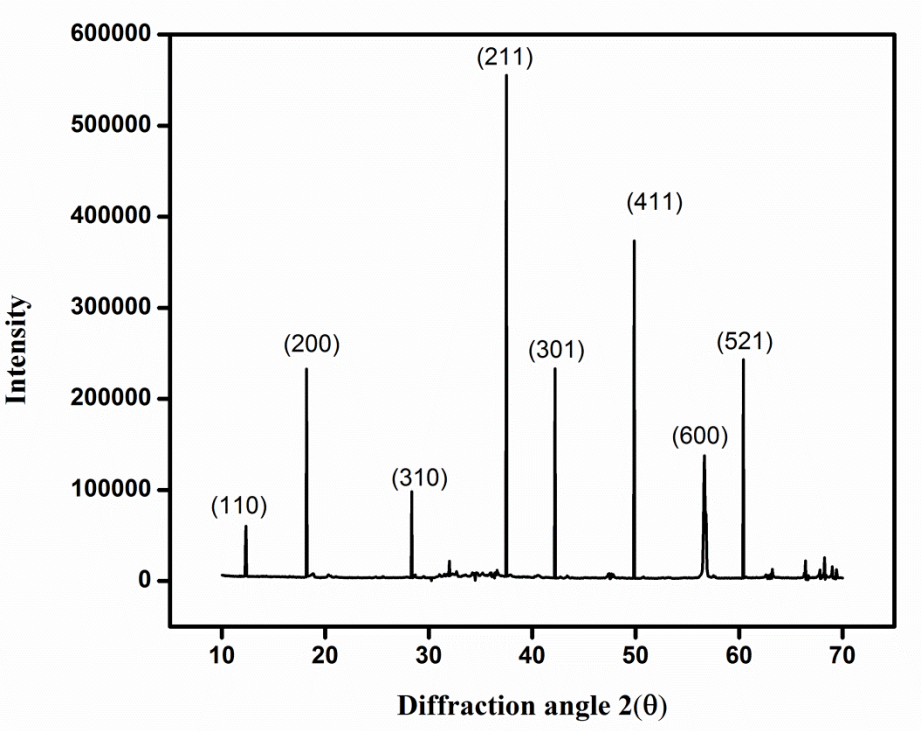

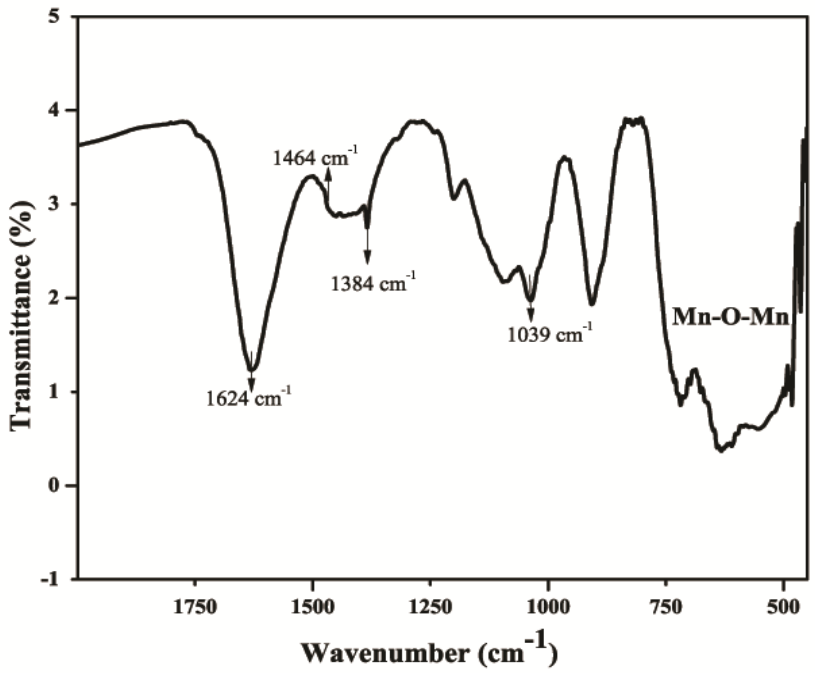

b) FTIR

eISSN: 2395-1648

INDEX COPERNICUS INTERNATIONAL

ICV 2014: 53.07
Standardized Value: 5.71

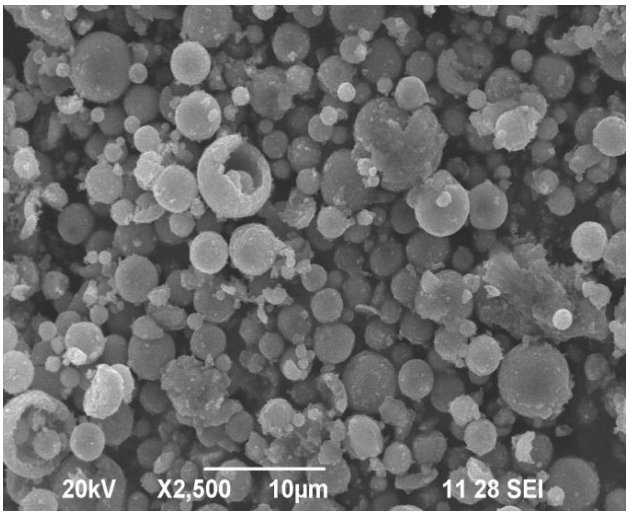

c) SEM

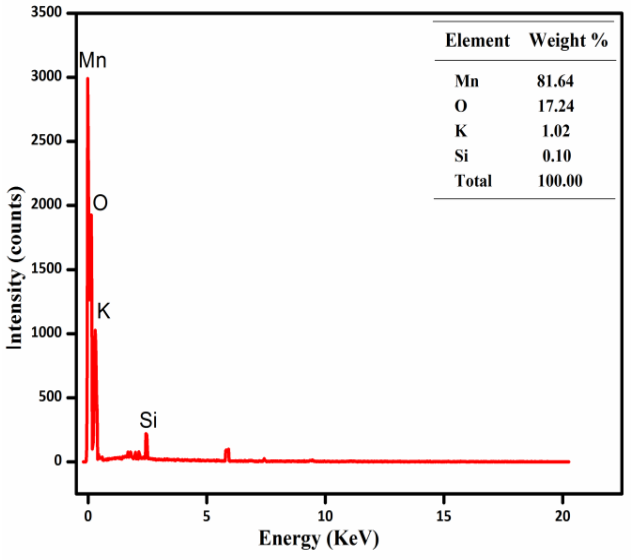

d) EDAX

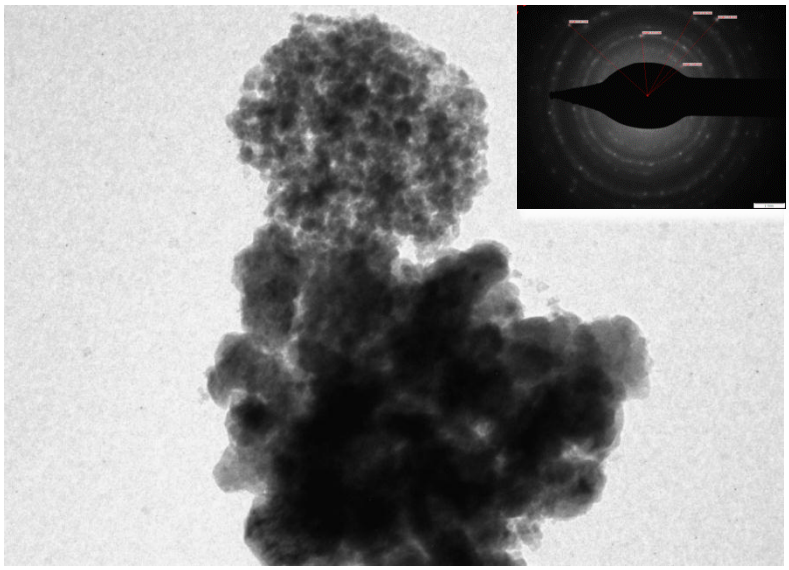

e) TEM

Fig.3. Characterization of α-MnO_2 nanoparticles a) XRD pattern, b) FTIR spectra, c) SEM image, d) EDAX pattern and e) TEM and SAED image pattern (inset).

eISSN: 2395-1648

INDEX COPERNICUS INTERNATIONAL

ICV 2014: 53.07
Standardized Value: 5.71

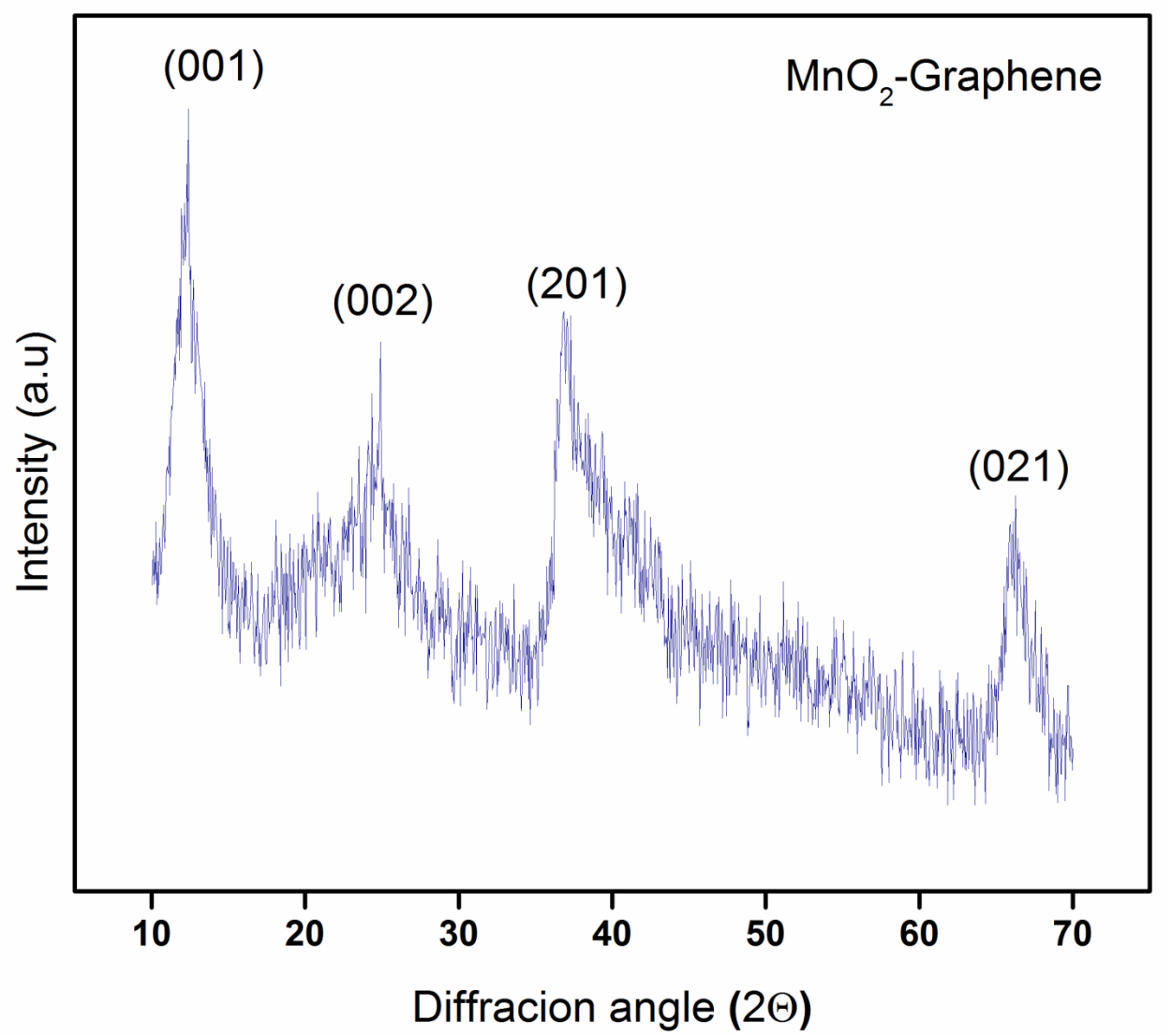

Fig. 4 XRD pattern of MnO_2-Graphene composite

eISSN: 2395-1648

INDEX COPERNICUS INTERNATIONAL

ICV 2014: 53.07
Standardized Value: 5.71

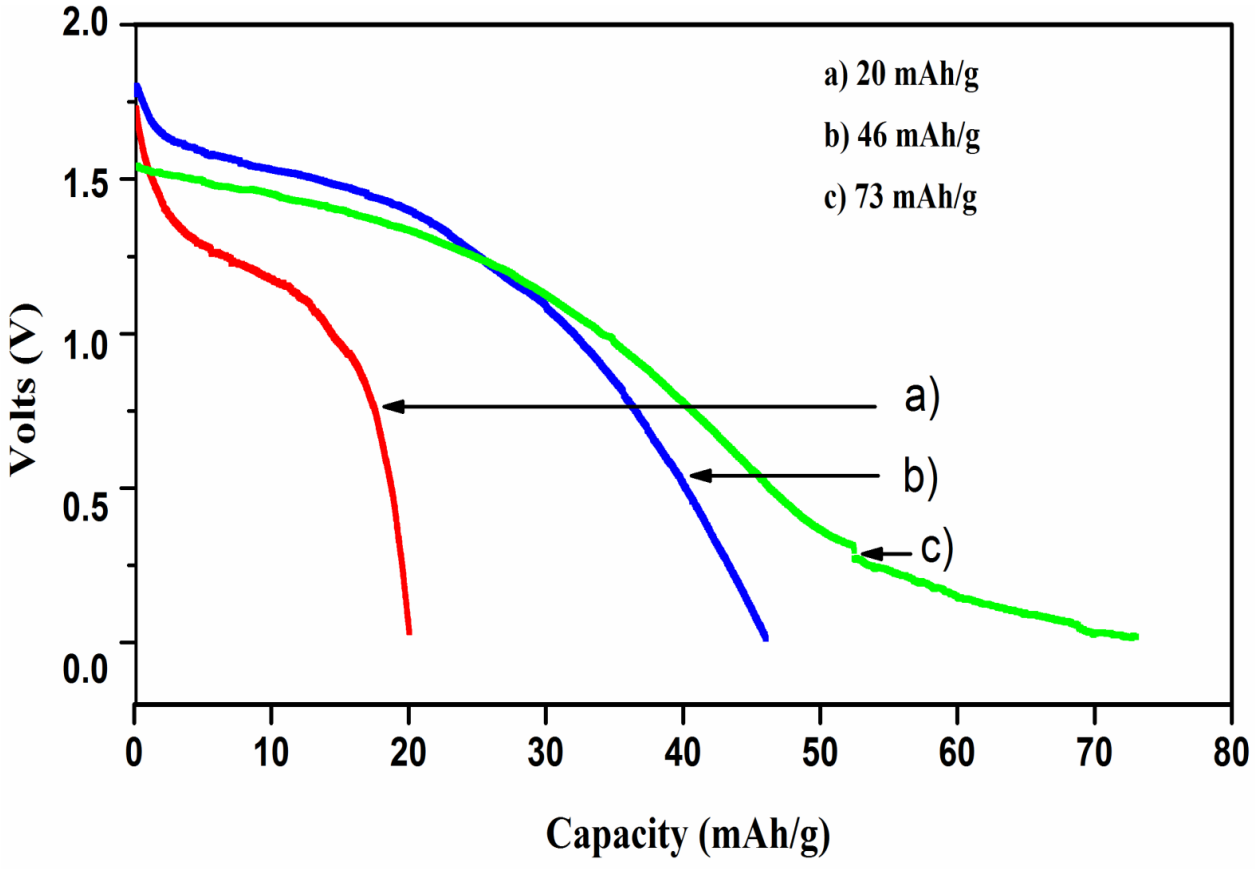

Fig.5. Comparison of voltage *versus* capacity curve of α-MnO_2 nanoparticle cathode in Mg primary electrochemical cell at a current rate of 1 mA (~C/300), b) 5 mA (~C/60), and c) 10 mA (~C/30)

eISSN: 2395-1648

INDEX COPERNICUS INTERNATIONAL

ICV 2014: 53.07
Standardized Value: 5.71

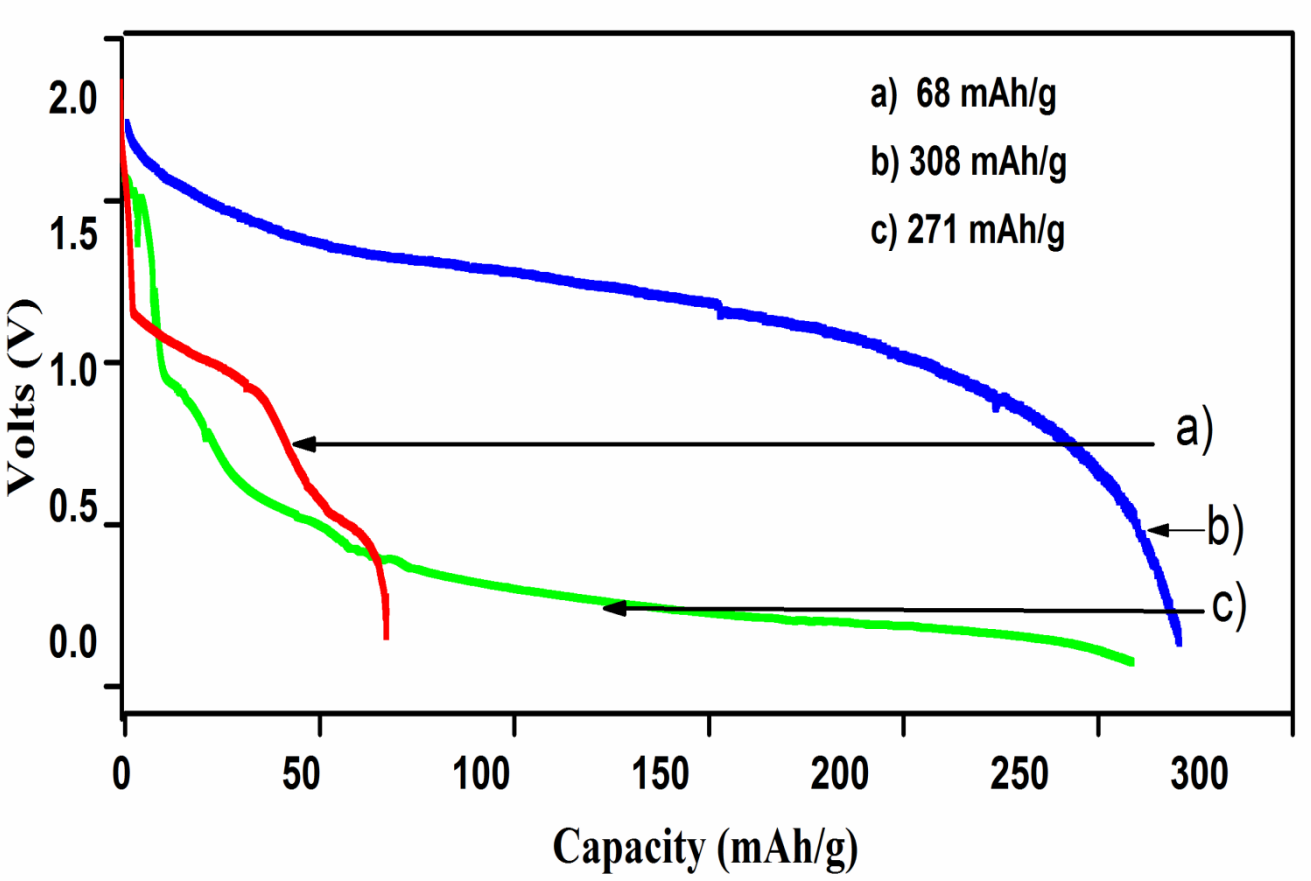

Fig.6.Comparison of voltage *versus* capacity curve of α-MnO_2-graphene cathode in Mg primary electrochemical cell at a current rate of a) 1 mA (~C/300), b) 5 mA (~C/60), and c) 10 mA (~C/30)

eISSN: 2395-1648

INDEX COPERNICUS INTERNATIONAL

ICV 2014: 53.07
Standardized Value: 5.71